



Chip formation and morphology in cryogenic machining of Al-SiC composites

Petr Mašek¹ · Nageswaran Tamil Alagan^{2,5} · Vladimír Mára³ · Samuel A. Awe⁴ · Emeka Nwabuisi⁵ · Pavel Zeman⁶

Received: 25 October 2024 / Accepted: 27 February 2025
© The Author(s) 2025

Abstract

This study investigated the influence of cryogenic cooling on chip formation and morphology during the turning of aluminum–silicon carbide (A359/SiC-20wt%) composites using an uncoated tungsten carbide cutting tool. The primary objective was to enhance the cutting conditions and improve the overall efficacy of the machining process for aluminum composite materials. Compared with dry machining, cryogenic cooling significantly altered the chip formation process, producing shorter and less curled chips at all tested cutting speeds. The rake and dual cooling strategies proved to be the most effective in terms of chip breakability, despite the relatively unchanged tool-chip contact length (chip ratio increased up to 25% and chip curl increased up to 20%). Cryogenic cooling also led to a reduction in average chip thickness, particularly with the dual cooling strategy, contributing to improved material removal efficiency. Microstructural analysis revealed that under cryo-cooling conditions, the hard SiC particles were distributed more uniformly within the chips, in contrast to the particle redistribution along the shear bands observed in dry cutting. Chip separation is primarily facilitated by the formation and propagation of cracks and microcracks along the matrix-particle interface, leading to noticeably frayed chip edges and improved breakability. The study also examined the effects of cutting speed and cooling strategy on chip characteristics, such as chip curl diameter, average chip thickness, chip compression ratio, and shear angle. For example, the chip curl diameter decreased by 18% with cutting speed and the shear angle increased by 16%. These findings contribute to the understanding of machining aluminum matrix composites under cryogenic conditions and provide insights for optimizing cutting parameters to enhance the machining performance, tool life, and surface quality.

Keywords Chip morphology · Chip contact area · Cryogenic cooling · Flank cooling · Turning · Aluminium matrix composite

✉ Petr Mašek
P.Masek@rcmt.cvut.cz
<http://rcmt.cvut.cz/home/en>

- ¹ Department of Production Machines and Equipment (RCMT), Faculty of Mechanical Engineering, Czech Technical University in Prague, Prague, Czech Republic
- ² Innovation and Technology, Hydro Extruded Solutions AB, Extrusion Europe, Finspång, Sweden
- ³ Department of Materials Engineering, Faculty of Mechanical Engineering, Czech Technical University in Prague, Prague, Czech Republic
- ⁴ Automotive Component AB, Floby, Sweden
- ⁵ Department of Engineering Science, University West, Trollhättan, Sweden
- ⁶ Department of Machining, Process Planning and Metrology, Faculty of Mechanical Engineering, Czech Technical University in Prague, Prague, Czech Republic

1 Introduction

Composite materials are currently used in various industries (particularly the construction, military, automotive, and aerospace industries) owing to their excellent specific properties such as strength or stiffness to weight ratio, increased wear resistance, low thermal expansion coefficient, high thermal conductivity, and ability to absorb energy or dampen vibrations [1–3]. Composites are multiphase materials because they usually consist of two or more constituents that exhibit significantly different physical and mechanical properties. The synergistic effect of the matrix and filler creates unique properties that the individual constituents do not possess. Matrix surrounds and binds reinforcement, provides geometrical stability, transfers the load on the reinforcement, protects the filler against environmental effects, and determines the surface quality. In contrast, high-strength filler is the

main load-bearing element. Fiber-reinforced (glass, carbon, aramid, boron) and particle-reinforced (metallic, ceramic) composite materials with various matrix types (polymer, metallic, ceramic) are the most commonly used composites for engineering applications [4, 5]. However, the addition of reinforcements to relatively easy-to-machine materials (matrices) transforms them into difficult-to-machine materials. Reinforcement significantly increases the abrasiveness of the composite material; however, some weaknesses of the matrices are preserved, such as low-temperature resistance (polymers) or brittleness (ceramics). The inhomogeneity of the composite material causes unpleasant post-machining quality problems, such as delamination and fiber or particle pull-out [6, 7].

One of the progressively used particulate metal matrix composites (MMC) is based on an aluminum matrix reinforced with dispersed silicon carbide particles (Al/SiC_p), which benefits from the combination of hard, stiff, but brittle load-bearing ceramic SiC particles with a ductile and low-density aluminum matrix. These types of composites are characterized by their hardness, resistance to abrasion, wear, and corrosion, and low cost [8]. Their mechanical properties can be controlled by changing the distribution, size, shape, or volume fraction of SiC particles [9]. However, owing to the hard and abrasive SiC particles, Al/SiC_p is considered a difficult-to-cut material. The contact of Al/SiC_p with the tool cutting edge results in abrasive wear of the tool, which significantly reduces the tool life, degrades the surface quality of the machined part, and increases the cutting force and cost [10, 11]. The applications of Al matrix composites include automotive components (pistons, pushrods, brake components), brake rotors for high-speed trains, bicycles or golf clubs, and high-voltage electrical cables [12].

During the machining process, the friction between the tool and MMC workpiece contact surfaces leads to a substantial increase in temperature. As the temperature increases, the SiC particles exhibit a greater propensity to absorb energy and consequently decrease the machining efficiency. With an increased SiC fraction, higher temperatures are concentrated on the surface of the workpiece owing to reduced heat conduction and dissipation. Abrasion of the SiC reinforcement results in material loss from the flank and edge of the tool. The increase in temperature caused by friction leads to secondary adhesion [13, 14]. However, inadequate heat dissipation results in substantial tool deformation and the formation of a built-up edge (BUE) on the tool surface, leading to deterioration of the workpiece surface and reduced tool life [15]. Cryogenic cooling results in temperature reduction at the incision site, thereby potentially inhibiting the formation of BUE, as corroborated by a previous study [16]. Nevertheless, the application of cryogenic cooling alone may prove insufficient if it induces inappropriate alterations in the conditions, as demonstrated in the

Laghari study [17]. This necessitates the use of an appropriate coolant capable of reducing the tool temperature and enhancing its longevity and surface integrity. Among the various cooling techniques, including flood, air, minimum quantity lubrication (MQL), and high-pressure cooling systems, cryogenic cooling (LN₂) has demonstrated superior suitability for machining difficult-to-cut materials owing to its enhanced capacity for rapid heat reduction, non-toxicity, environmental compatibility, and chemical inertness (which mitigates the potential for tribochemical reactions) [18]. The impact of cryogenic coolants on chip morphology and formation mechanisms in aluminum matrix composites has not been comprehensively investigated. Elucidating the relationship between cryogenic cooling strategies and chip formation can provide valuable insights for optimizing machining parameters to enhance performance.

Duan et al. [19], in their study on the effect of cooling and lubrication conditions on tool wear in turning of Al/SiC_p , asserted that the application of cryogenic coolant increased the thermal impact and scratch effect on the tool face due to SiC presence, which consequently increased tool breakage. However, they observed that MQL increased the tool life and resulted in lower flank wear. Joysula et al. [20] investigated the sustainable machining of metal matrix composite utilizing liquid nitrogen and observed that cryogenic cooling reduces surface roughness, tool wear, and cutting temperature. Aurich et al. [21] examined the influence of reinforcement and cutting conditions on the surface layer of the workpiece and noted that the feed rate was the primary parameter affecting the surface layer, as it decreases the tensile stress on the workpiece but negatively impacts surface quality. Ghoreishi et al. [22], in their evaluation of tool wear in high-speed face milling of Al/SiC_p MMC, observed that the presence of SiC particles in the aluminum matrix composite causes severe tool wear and that the application of a cryogenic coolant can reduce tool wear. The cryogenic coolant demonstrated superior efficacy in achieving enhanced surface integrity during the drilling of Al/SiC compared to MQL, as evidenced by the evaluated parameters of surface roughness and burr height. However, an increase in microhardness was observed during experimental investigations [23].

In the machining operation, the cutting tool edge interacts with the workpiece material, causing it to separate through plastic deformation. This process allows the removed material to glide along the rake surface of the cutting tool. The deformed portion of the material that is removed is known as a chip [24, 25]. The type and morphology of the chips produced during machining depend on the cutting parameters (cutting speed, feed, and depth of cut), workpiece material, cutting environment, tool geometry, and material [24, 26]. Chip formation and breakability (the ability of the chip formed during machining to break off from the workpiece)

play key roles in determining the surface quality, tool life, machining performance, and cost [20, 25]. Chip formation during machining processes was also investigated by Abbas et al. [27], who observed that chips fragmented into shorter lengths under cryogenic cooling conditions. They further postulated that this phenomenon was correlated with the increased hardness observed as a result of the cooling process. Various types of chips can be generated during the machining process. For instance, elongated, continuous ribbon-like chips may present operational challenges and necessitate process interruptions. This phenomenon reduces productivity, increases machining time and cost, adversely affects machine performance, poses a potential hazard to the operator, and can negatively affect the surface quality. Consequently, it is imperative to study and obtain desirable chip breakability during the machining process. Chip breakability depends on the workpiece material, cutting conditions, tool geometry, cooling conditions, and chip curling [28]. Chip curling is significant because of its role in separating chips from the tool surface. This separation is crucial because the duration of chip contact with the tool surface is directly proportional to the heat transfer from the chip to the tool [29]. Chip curling manifests in two forms: natural and forced. In natural curling, the chip exits the rake face without encountering any obstruction or obstacles. Conversely, in forced curling, the chip interacts with an obstacle such as a tool breaker, workpiece, or the face of the tool [30]. The presence of this obstacle aids chip curling, which in turn aids chip breakability and influences the surface quality of the machined workpiece.

Dabade et al. [34] in their work observed that in Al/SiC_p, the number of curls that the chip makes before breaking depends on the number of reinforcement particles present; as the reinforcements increase, chip curling decreases owing to the brittleness of the reinforcements. Wu et al. [35] observed that the brittle fracture of the SiC particles in the cutting path can form large cavities and the deformed Al matrix forms the smooth surface of the workpiece by covering the cavities. Al matrix deforms along the shear plane and serrated chip segments are separated along the plane with clustered particles. Xiang et al. [31] observed that during the high-speed cutting of Al/SiC_p, chip formation was induced by the high shear strain in the primary deformation zone, the difference in flowability of the free and back surfaces of the chip, and the instabilities of plastic deformation and damage promoted by adiabatic shear localization, which led to the formation of mixed serrated chip morphologies. Nakayama et al. [32] observed that chip breakage occurs when the strain on the chip increases beyond a certain critical value.

Table 1 presents a summary of various recent machining studies that have utilized cryogenic coolants or conventional cooling media. Based on this table and the preceding text, it can be concluded that the selected topic is highly contemporary and has not yet been fully elucidated. A comprehensive description of the behavior of MMC materials during cryogenic cooling through discrete studies is necessary. The potential advantage lies in the possible enhancement of productivity and quality while simultaneously reducing machining costs if the process is thoroughly characterized. However, considering the material properties, machining

Table 1 Summary table of the most important technological references and their aim

Machining method	Author	Ref. no	Year	Cryogenic cooling	Chip formation	Additional categories
Drilling	Abbas et al	[24]	2024	Yes	Yes	Chip hardness under cryogenic cooling
	Chakravarthy et al	[23]	2022	Yes	Yes	Effect of nanoparticles on surface integrity
Milling	Ghoreishi et al	[22]	2019	Yes	Yes	Tool wear
	Sivalingam et al	[16]	2023	Yes	Yes	Hybrid metal composites
	Wu et al	[2]	2019	No	Yes	Fracture modelling of composites
	Wu et al	[31]	2019	No	Yes	Subsurface damage
Turning	Duan et al	[19]	2019	Yes	No	Tool wear
	Josyula et al	[27]	2016	Yes	Yes	Sustainable machining
	Aurich et al	[21]	2016	No	Yes	Effect of reinforcement on surface
	Xiang et al	[32]	2021	No	Yes	High-speed machining
	Masek et al	[6]	2021	Yes	Yes	Influence of temperature on cutting mechanisms
	Nakayama et al	[33]	1962	No	Yes	Study on chip breaking
	Hung et al	[15]	1998	No	Yes	Chip formation mechanisms
Multiple methods	Muthukrishnan et al	[34]	2008	No	Yes	Machining of metal composites
	Laghari et al	[17]	2023	Yes	No	Sustainable cooling
General machining	Chen et al	[10]	2020	No	Yes	Conventional and non-conventional methods
	Chawla et al	[9]	2001	No	Yes	Mechanical properties of composites
High-speed machining	Xiang et al	[32]	2021	No	Yes	Cutting condition modeling
Laser turning	Przestacki et al	[1]	2016	No	Yes	Surface layer structure

characteristics, and prior research findings, it is imperative to investigate the relationship between the machining characteristics and chip formation in Al/SiCp composites. By examining this relationship, it may be feasible to optimize the cutting conditions and enhance the overall performance of the machining process for aluminum composite materials. Consequently, this study aims to establish the impact of cutting speed and various cryogenic cooling strategies on the alterations in the microstructure, chip morphology, and key characteristics of Al/SiCp. The findings of this investigation will contribute to advancements in machining technologies for MMC and provide insights that ultimately influence efficiency, tool life, and surface quality when addressing the challenges presented by composite materials.

2 Materials and methods

2.1 Workpiece and cutting tool

The material used in this study was an aluminum matrix composite brake rotor (Fig. 1), which comprised aluminum A359 alloy with a chemical composition of AlSi9Mg0.6, reinforced with 20 wt% silicon carbide particles with an average particle size of 18 μm . This specific material was chosen for investigation owing to its widespread usage, low cost, high strength, and capacity for large-scale production. The blank rotor workpiece was manufactured using the squeeze casting method and supplied by Automotive Components Floby AB, Sweden. A photograph of the test piece

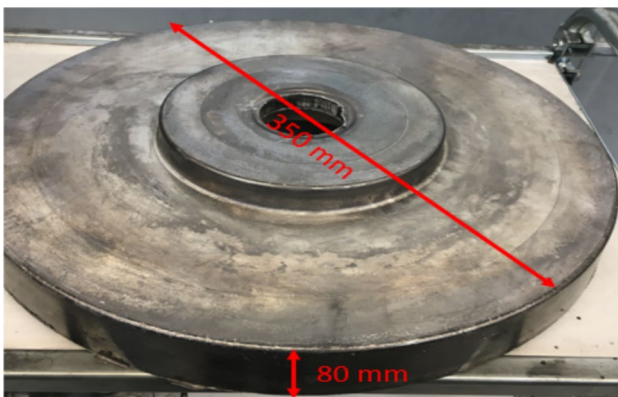


Fig. 1 Photograph of squeeze-cast MMC blank rotor

is shown in Fig. 1. The dimensions of the blank MMC rotor were as follows: thickness, 80 mm; outer diameter, 350 mm; and inner diameter, 80 mm. The bulk hardness of the material was determined to be 75 ± 9 HBW by applying a 750 kg load with a 5 mm diameter steel ball for 10 s on a Brinell hardness tester. Table 2 provides further details of the physical and mechanical properties of the test material.

The cutting tool employed was an uncoated carbide tool with a rhombic shape and grade designation of K68, with an ISO designation of CNMA120408. The detailed specifications of the cutting tool are presented in Table 3. This specific grade of cutting tool comprises tungsten carbide and cobalt as its primary constituents, which are alloyed to form fine-grained structures. Owing to its high resistance to abrasive wear, this grade of cutting tool is recommended by cutting tool manufacturers for machining difficult-to-cut materials. The suitability of uncoated rhombic cemented carbide grades for rough machining operations is attributed to their controlled wear rate and self-sharpening action, which allow for efficient and effective performance during these tasks [33]. Consequently, a rhombic carbide tool with dimensions identical to those used in the industry was selected for the experiments. The tool holder used was a Kennametal DCLNL20X12 JETI equipped with internal channels featuring two coolant nozzles aimed at the rake and flank faces of the insert. The diameters of these nozzles were 0.8 mm and 1.4 mm. The geometrical configuration of the insert secured within the tool holder comprised a rake angle (γ_o) of -6° , an edge inclination (λ_s) of -5° , and a major cutting-edge angle (κ_r) of 95° .

2.2 Cryogenic and machining setup and process

The experimental setup for the machining and cooling procedures is illustrated in Fig. 2a and b. Four experimental

Table 3 Insert nomenclature

Insert cutting edge length [mm]	12.7
Insert thickness [mm]	4.763
Corner radius [mm]	0.8
Insert hole size [mm]	5.16
Clearance angle [$^\circ$]	0
Type of insert	Uncoated carbide
Insert shape	Rhombic 80°

Table 2 Mechanical properties of workpiece material

Density (g/cm^3)	Yield strength (MPa)	Ultimate tensile strength (MPa)	Elongation (%)	Young modulus (GPa)	Poisson's ratio (-)	Fracture toughness ($\text{MPa}\cdot\text{m}^{1/2}$)
2.71	138.7	178.3	1.9	109	0.31	15.9

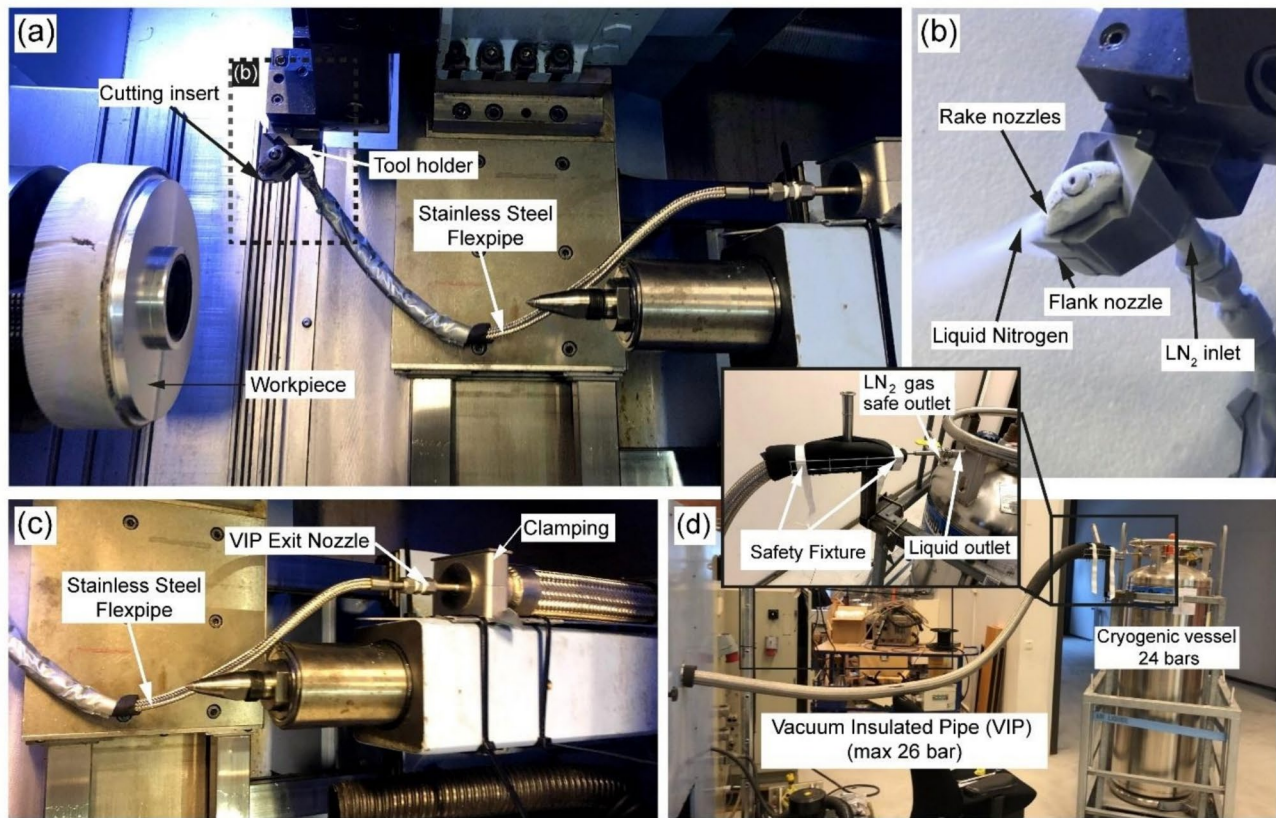


Fig. 2 Cryogenic experimental setup for face turning (a) machining process setup, (b) LN_2 from both rake and flank nozzles of the tool holder, (c) exit of the VIP nozzle connected to the flex pipe, (d)

LN_2 tank connected to the VIP (the magnified view—a custom-made safety fixture for the VIP)

conditions, comprising dry machining and three cryogenic configurations, were employed in this investigation. Dry machining was conducted at an ambient temperature of 23 °C, where no external cooling was applied. In contrast, for cryogenic cooling subzero conditions, liquid nitrogen (LN_2) was used as the coolant. LN_2 rapidly absorbs heat upon contact with the machining zone. As it evaporates, it undergoes a phase change from liquid to gas, creating a localized cooling effect. The medium was contained in a 200 L gas cylinder equipped with a pressure cap valve (Fig. 2d). A valve positioned at the outlet of the liquid–nitrogen cylinder regulated the gas flow into the system. The valve was connected with a vacuum-insulated pipe (VIP) to the exit nozzle in the lathe machine chamber and with a flexible pipe to the tool holder (Fig. 2c). The medium was applied through a rake and/or flank nozzle, which led to a distinction between rake, flank, or both (dual) cooling strategies. The coolant density was 1.251 kg/m^3 and was maintained at a temperature of -196 °C and a pressure of 20 bars.

The machining process involved a face-turning operation with a setup consisting of an STM 2000 CNC lathe machine (manufactured by STOREBRO Machine Tools

AB). The workpiece was secured to the chuck via its internal diameter and dynamically balanced to prevent wobbling or irregular rotation. The cutting rate was maintained constant for the duration of cutting. The tool holder was fastened to the upper turret, which was linked to the coolant distribution network. The effect of cutting speed in combination with various coolant strategies on the chip formation process was studied. The depth of cut and feed were kept constant, while the cutting speed was varied at three levels. The spiral cutting length (SCL) was calculated and used in machining according to [36, 37]. The cutting parameters used in the experiment are summarized in Table 4.

Four different experiments under different cooling conditions were performed at each cutting speed.

- Dry condition,
- Cryogenic condition (LN_2) at the rake face,
- Cryogenic condition (LN_2) at the flank face,
- Cryogenic conditions (LN_2) at rake and flank faces.

The used tool and chips formed under each condition were collected and analyzed. The chip structure, form,

Table 4 Cutting parameters and cooling conditions for tests

Parameters	Description
Cutting speed (m/min)	150, 180, 210
Feed rate (mm/rev)	0.3
Depth of cut (mm)	0.5
Spiral cutting length (SCL) (m)	35
Cooling conditions	Dry, rake, flank, dual
Nozzle orifice diameter (mm)	0.8 (rake), 1.4 (flank)

and dimensions were investigated. Microstructural analysis of the chips was performed to observe the changes that occurred in the material after machining. Important parameters such as chip thickness, chip compression ratio, chip curl diameter, tool-chip contact length, and shear angle were evaluated to provide data for analysis and comparison.

2.2.1 Enhancing safety and risk mitigation in liquid nitrogen operations

The safe handling of liquid nitrogen is essential to prevent operational risks associated with extreme cryogenic temperatures, rapid gas expansion, and potential oxygen displacement. Key risk mitigation strategies include the following:

- Proper training and handling procedures—Personnel must be well-trained in cryogenic safety, including safe transfer, storage, and usage protocols.
- Adequate personal protective equipment (PPE)—Cryogenic gloves, face shields, insulated aprons, and protective footwear should be worn to prevent cold burns and frostbite.
- Ventilation and oxygen monitoring—Liquid nitrogen vaporizes rapidly, posing an asphyxiation hazard in confined spaces. Adequate ventilation and oxygen sensors placed close to the operation/personal are necessary to ensure safe atmospheric conditions.
- Safe storage and transportation—Insulated, pressurized containers must be used, and storage areas should be free from combustible materials. Proper labelling and transport protocols should also be followed.
- Controlled use in laboratories and industry—Equipment designed for liquid nitrogen applications should be inspected regularly, and emergency protocols must be established for potential leaks or exposure incidents.

By integrating these measures into operational protocols, organizations can significantly reduce risks associated with liquid nitrogen, ensuring both workplace safety and compliance with industry regulations.

2.3 Measurement methods

2.3.1 Chip formation analysis

The configuration, shape, and type of chips formed were examined using an Olympus SZX9 microscope at multiple magnifications. The parameters of chip thickness (t_c), chip curl diameter (d_o), and tool-chip contact area length (TCC_{length}) were evaluated, as shown in Fig. 3. Ten different chips were analyzed for each machining condition. Five values for each parameter were measured for each chip.

The chip compression ratio (r_c) and shear angle (φ) were determined based on the measured data from the chip microstructure analysis. The chip compression ratio served as an indicator of the plastic deformation intensity of the material. This is the ratio between the undeformed chip thickness (t) and chip thickness (t_c), as shown in Eqs. 1 and 2 [36, 37] and Fig. 4a. Next, the shear angle was evaluated as one of the most important parameters defining the chip formation process. The shear angle is the resultant combination of the two approaches to reduce evaluation inaccuracies. First, it was calculated from the measured chip thickness using Eq. 3 [38]. Next, the values of the segment orientation angle were determined from the chip images (Fig. 4b). The angle was then calculated using Eq. 4. Ten orientation values were obtained from each chip, and three chips were evaluated for each cooling and cutting condition. Eventually, the average value of both approaches was determined as the resultant shear angle.

$$r_c = t/t_c \quad (1)$$

$$t_c = t_{min} + (t_{max} - t_{min})/2 \quad (2)$$

$$\varphi = \arctg(r_c \cos \gamma / (1 - r_c \cos \gamma)) \quad (3)$$

$$\varphi = 90^\circ - \Phi \quad (4)$$

where γ is the rake angle and Φ is the angle of the segment orientation.

2.3.2 Microstructural analysis

Metallographic samples were extracted from the friction ring cross-section of the work material (Fig. 1) and prepared for microstructural examination. Before the analysis, the samples were prepared using the standard metallographic procedure: grinding with SiC papers up to #4000 grit, pre-polishing with non-drying fumed silica (SiO₂) suspension (0.25 μ m), and final polishing with acidic alumina (Al₂O₃) suspension (0.05 μ m). The

Fig. 3 Measurement method for (a) chip curl diameter, (b) chip thickness, (c) tool chip contact length on the tool rake face

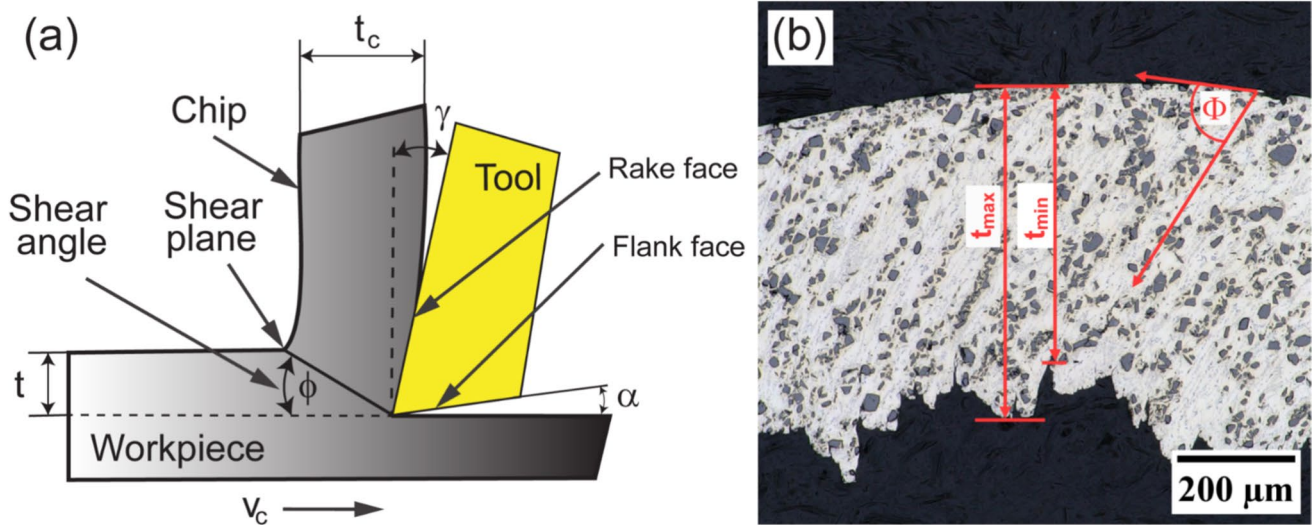
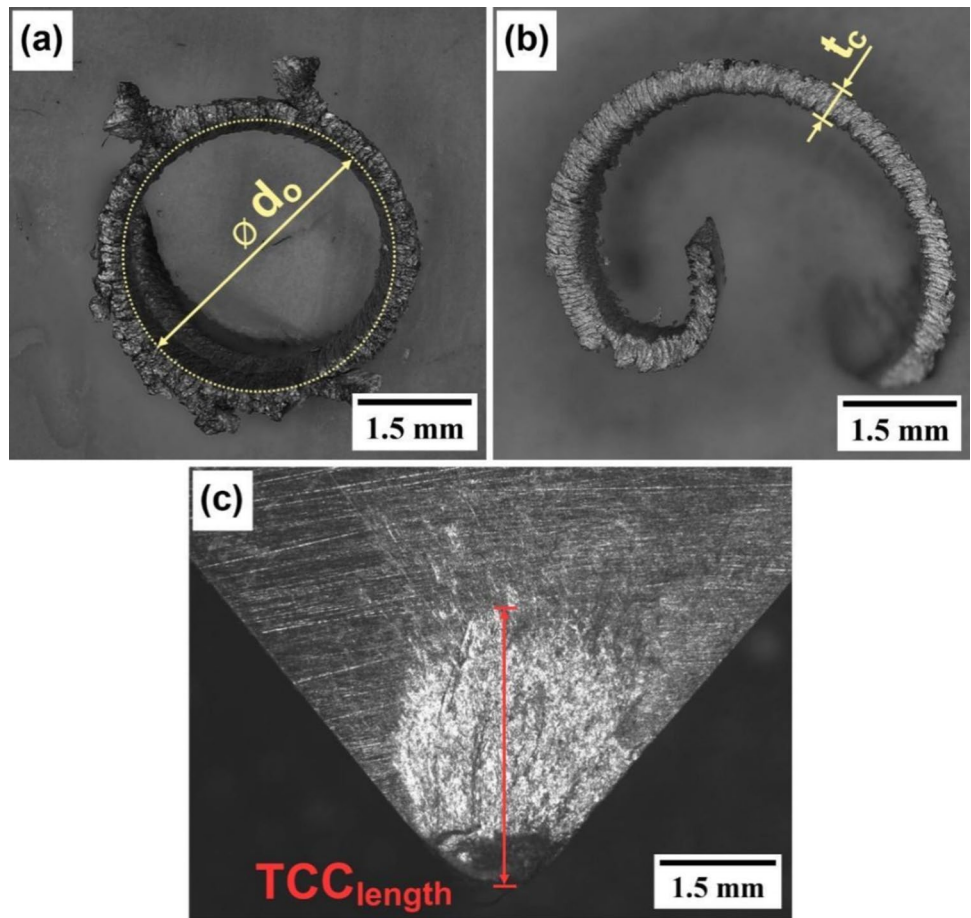


Fig. 4 (a) Schema of turning process, (b) chip characteristic evaluation

microstructure of the work material and the morphology of the chips were studied using a light optical microscope (LOM) ZEISS Imager M2m Axio, Olympus SZX9, and Olympus DSX1000. Detailed microstructural analysis was

performed using a HITACHI TM 3000 and JEOL JSM 7600-F scanning electron microscope (SEM) equipped with secondary (SE) and backscatter detectors (BSE). The phases present in the microstructure were identified by

energy-dispersive X-ray spectroscopy (EDXS) using an SDD Oxford X-Max 80 mm² detector.

3 Results and discussion

3.1 Chip morphology, length, and breakability

The cutting speed and cooling strategy have a significant impact on chip morphology, length, and breakability. The work material exhibited a combination of brittle behavior from hard particles and ductile and adhesive properties from the matrix. Despite the presence of frayed edges, chips with long continuous spiral shapes were formed at all cutting speeds under dry conditions.

In general, the use of cryogenic coolants results in notable differences in the length, curl dimensions, and overall shape of the chip, as illustrated in Fig. 5. Both sides of the

chip exhibited a significant degree of frailty. Consequently, the strength of the chip was lower, and its fragmentation and susceptibility to breaking were higher. Dry machining resulted in tubular short chips approximately 30–40 mm in length, regardless of the cutting speed used (see the area in Fig. 5a). Cryo-cooling supports chip breakability (length of chips 10–20 mm). The influence varied with the cooling strategy and cutting speed. The rake and dual strategies yielded the shortest number of chips. At lower speeds, the chips were narrower and exhibited less deformation (indicating a higher pitch of the chip threads). This indicates that the chips were properly cooled with a low-temperature gradient, as shown in Fig. 5c. However, the chips were slightly longer and curled more with increasing cutting speed as the cutting temperature increased, as shown in Fig. 5b.

A comparative analysis of the backside (tool-side) of the chips and their fragmentation is shown in Fig. 6. The regions of higher luminosity indicate smoother surfaces generated

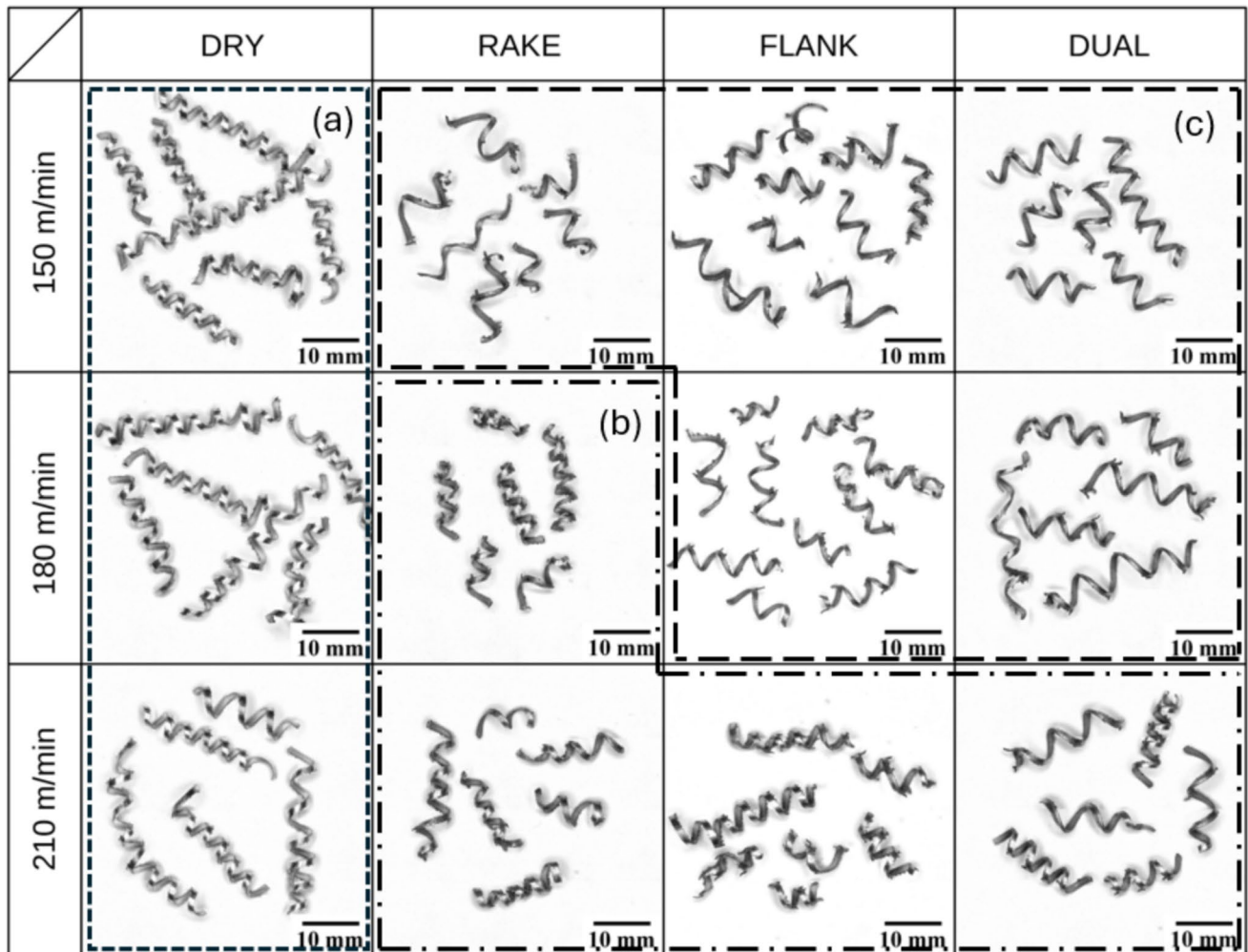


Fig. 5 Effect of cooling strategy and cutting speed on chip length on breakability: (a) tubular chips during dry machining, (b) shorter tubular chips using cryo-coolant, and (c) narrower and shorter tubular chips using cryo-coolant

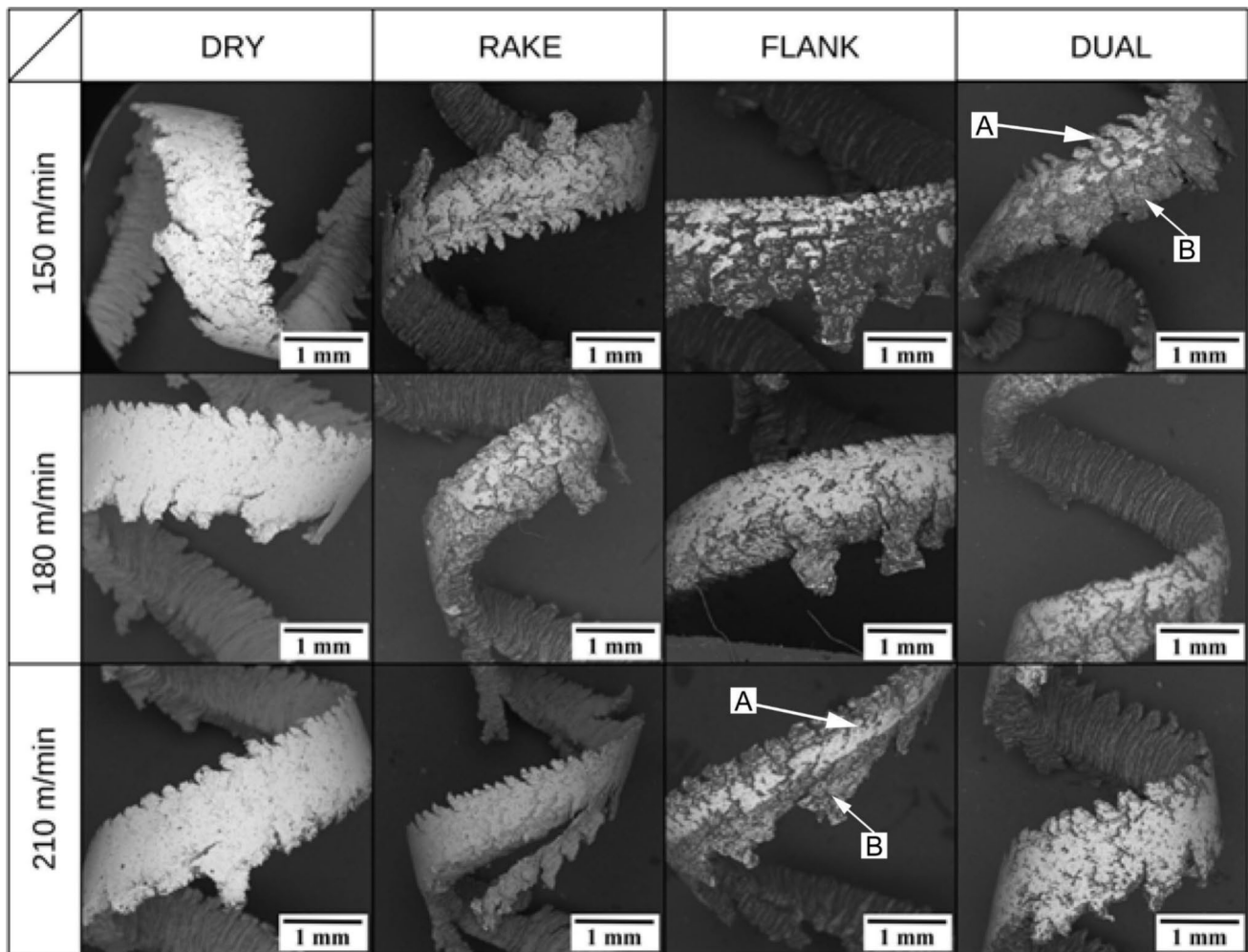


Fig. 6 Effect of cooling strategy and cutting speed on chip morphology; A—sliding marks; B—sticking imprints

within the sliding region during the final phase of the tool-chip contact, as exemplified by area “A” in Fig. 6. This occurred during the dry and flank cooling strategies, particularly when the cutting temperature was relatively high. In contrast, the increased efficiency of the cooling system and the lower temperature at the tool-chip interface led to greater adhesion between the tool and chip, as evidenced by more pronounced sticking marks or impressions (e.g., area “B”). A similar occurrence was observed in a previous study conducted by Alagan et al. [37].

The SEM image of a representative chip generated under cryo-cooling conditions (“Rake,” 180 m/min) is shown in detail in Fig. 7. Based on the image depicted in Fig. 7a, one can observe the frayed edges of the chip and its segmentation, which indicates the presence of non-uniform SiC particles, reduced material cohesion, and diminished plasticity, ultimately resulting in a decreased capacity for shear deformation. Distinctions between the regions of sliding and sticking marks on the reverse side are evident in the image

on the right (Fig. 7b). A rough surface indicates significant adhesion at the tool-chip interface as the temperature is effectively reduced.

3.2 Chip characteristics

Effective management of chip characteristics is crucial for achieving efficient, secure, and top-notch machining processes. However, by focusing on chip formation, machinists can diagnose machining issues, optimize cutting conditions, and improve the overall process performance. The data gathered from the chips were examined to assess the chip curl diameter, tool-chip contact length, average chip thickness, chip compression ratio, and shear angle. The findings of these evaluations are summarized in Table 5. The chip curl diameter (d_c) exerts a significant influence on chip breakability because its reduction causes the chip to curl away from the rake face in either an upward or a sideways direction.

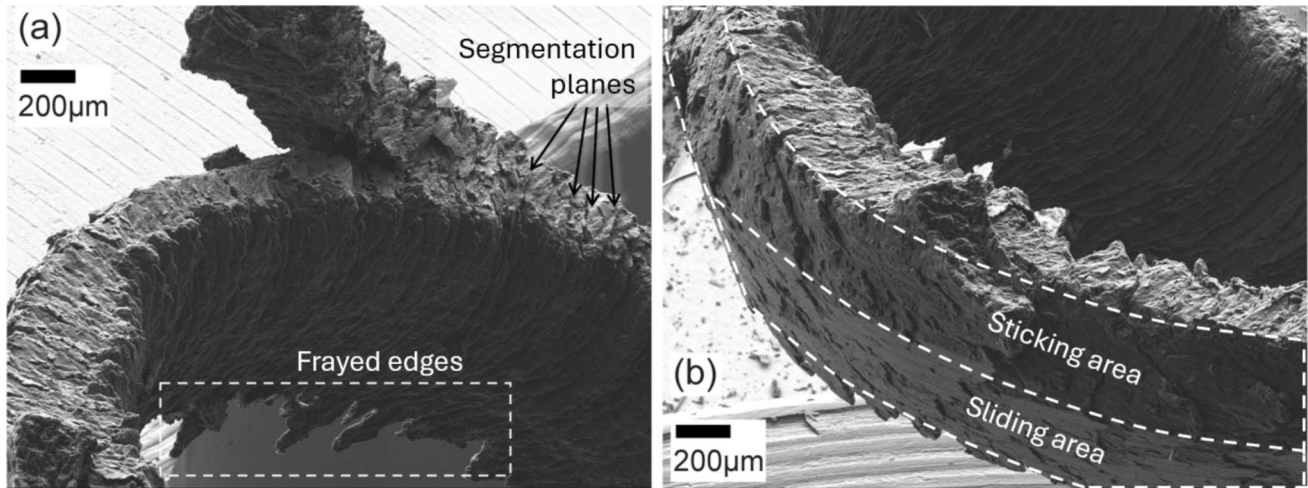


Fig. 7 Details of a chip (SEM): (a) free-surface view and (b) tool-side view

Table 5 The results of chip characteristics

Measured parameter	Coolant condition	Cutting speed [m/min]		
		150	180	210
Chip curl diameter d_c (mm)	Dry	5.74 ± 0.56	5.72 ± 0.48	4.48 ± 0.50
	Rake	7.32 ± 0.50	6.40 ± 0.50	6.03 ± 0.26
	Flank	7.21 ± 0.64	7.36 ± 0.60	5.98 ± 0.32
	Dual	7.33 ± 0.74	6.97 ± 0.28	6.41 ± 0.32
Tool-chip contact length TCC_{length} (mm)	Dry	1.00 ± 0.03	0.96 ± 0.02	0.95 ± 0.05
	Rake	0.98 ± 0.03	0.96 ± 0.01	0.94 ± 0.04
	Flank	1.00 ± 0.01	0.97 ± 0.04	0.95 ± 0.04
	Dual	0.97 ± 0.01	0.97 ± 0.01	0.97 ± 0.05
Average chip thickness t_c (mm)	Dry	0.61 ± 0.02	0.55 ± 0.05	0.50 ± 0.01
	Rake	0.61 ± 0.05	0.61 ± 0.02	0.60 ± 0.02
	Flank	0.56 ± 0.15	0.58 ± 0.01	0.51 ± 0.03
	Dual	0.56 ± 0.02	0.57 ± 0.03	0.55 ± 0.02
Shear angle φ (deg)	Dry	20.3 ± 2.9	27.9 ± 3.5	29.8 ± 3.1
	Rake	21.4 ± 5.2	22.1 ± 1.5	23.4 ± 2.4
	Flank	24.3 ± 1.6	25.8 ± 1.9	28.4 ± 1.6
	Dual	24.0 ± 4.5	24.1 ± 3.8	26.5 ± 2.2
Chip compression ratio r_c (-)	Dry	0.38 ± 0.08	0.42 ± 0.20	0.46 ± 0.06
	Rake	0.38 ± 0.16	0.38 ± 0.29	0.39 ± 0.29
	Flank	0.41 ± 0.19	0.40 ± 0.23	0.45 ± 0.09
	Dual	0.42 ± 0.20	0.41 ± 0.38	0.43 ± 0.15

This phenomenon results in a decrease in the tool-chip contact area and length, thereby enhancing chip breakability.

The curl diameter decreased with the cutting speed under dry conditions as the temperature and its gradient across the chip increased, as shown in Fig. 12a. These findings correlate with those of Yaman [39]. Subsequently, the parameter was significantly lower than that for all cryogenic cooling states. This corresponds to the aforementioned observation of the chip shape. There was a less pronounced effect of cutting speed on the course for all coolant conditions. The curl diameter decreased with rake, flank, and dual cooling, whereas the specific cryogenic cooling strategy did

not significantly influence the chip curl. According to the analysis of variance (ANOVA) test, both control factors (coolant and v_c) demonstrated statistical significance at a significance level of $\alpha = 0.05$. A substantial difference was observed between dry machining and coolant application (almost 20%), as illustrated in the main effect plot in Fig. 8. The results indicated an inverse relationship between the cutting speed and chip curl radius, with higher cutting speeds corresponding to smaller chip curl radii. In the tested range, up to 18% decrease of chip curl radius was found.

The average chip thickness was largely determined by the feed rate and cutting speed. However, the most significant

Chip curl rad versus Coolant; v_c					
Source	DF	Adj SS	Adj MS	F-Value	P-Value
Coolant	3	2.3878	0.79592	4.60	0.018
v_c	2	1.4178	0.70892	4.09	0.038
Error	15	2.5975	0.17316		
Lack-of-Fit	6	0.1738	0.02896	0.11	0.993
Pure Error	9	2.4237	0.2693		
Total	20	6.2548			

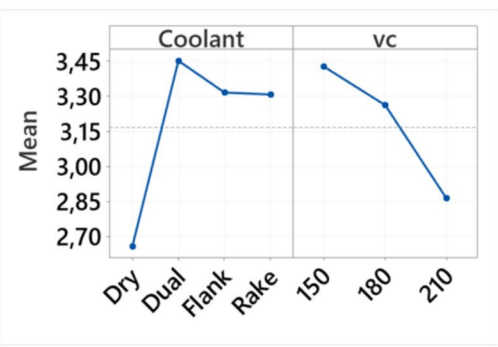


Fig. 8 ANOVA test for chip curl radius with main effect plot

factor was the work material and its behavior in the shear zone. When turning the aluminum matrix composite, it exhibited similar behavior in terms of chip thickness as homogeneous metals, with the average chip thickness decreasing with increasing speed. As the metal matrix exhibited increased plasticity in the primary shear zone, the width of the chip decreased and was oriented towards the rake face, as illustrated in Fig. 12. Similar observations were reported by Kaynak et al. [40].

In contrast, cryo-cooling resulted in the opposite effect. Specifically, the average chip thickness increased with the cutting speed for all cryo-cooling strategies, and no significant difference was observed in the cooling strategy. This behavior can be attributed to microstructural changes in the work material and lower chip temperatures. Moreover, higher adhesion occurs at the tool-chip interface. These conditions support the creation of a stable build-up edge and influence the chip formation process. Analysis of variance of the test results revealed low statistical significance ($\alpha=0.05$) for both control factors. It was not feasible to ascertain whether the coolant and cutting speed influenced the chip thickness (Fig. 9).

The chip compression ratio was influenced by the chip thickness, as demonstrated by the utilization of a constant feed in all experiments. Theoretically, this ratio should

decrease according to the mechanisms defined by Astakhov [41]. Upon the implementation of a cryocoolant environment, the ratio exhibited an increase of 40% at a cutting speed of 150 m/min. Nevertheless, no statistically significant difference was observed in the chip compression ratio when comparing the effects of the cutting strategy and flow direction at various cutting speeds, as indicated by the ANOVA test presented in Fig. 10. The main effect plot reveals a slight decrease in the chip compression ratio with cutting speed. The dual coolant increased the chip compression ratio up to 25%

The tool-chip contact length showed a decreasing trend with the cutting speed for all cooling strategies, as well as for dry conditions (Fig. 12c). This finding is consistent with previous observations on chip curl diameter (d_o) and the study of Storchak et al. [42]. No statistically significant variation was observed among the strategies at a specific cutting speed. However, the standard deviations for this measurement were relatively substantial. This finding was statistically validated using ANOVA (Fig. 11). The cutting speed was determined to be statistically significant based on the p -value. Consequently, these differences are inconclusive. The flank cooling strategy has a similar effect as the rake and dual methods. Hence, the dynamic effect of the rake cryocoolant on the chip and secondary shear zone

Chip thickness h_{Dc} versus Coolant; v_c					
Source	DF	Adj SS	Adj MS	F-Value	P-Value
Coolant	3	0.01879	0.006264	0.32	0.813
v_c	2	0.01428	0.007138	0.36	0.7
Error	27	0.53332	0.019753		
Lack-of-Fit	6	0.01244	0.002074	0.08	0.997
Pure Error	21	0.52088	0.024804		
Total	32	0.56601			

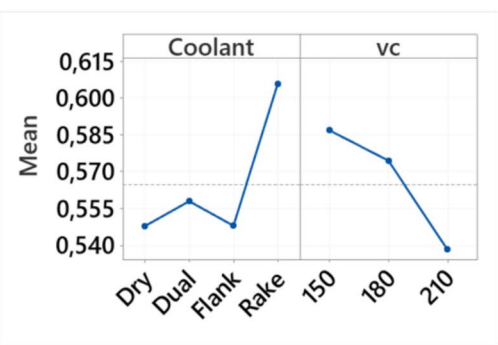


Fig. 9 ANOVA test for chip thickness with main effect plot

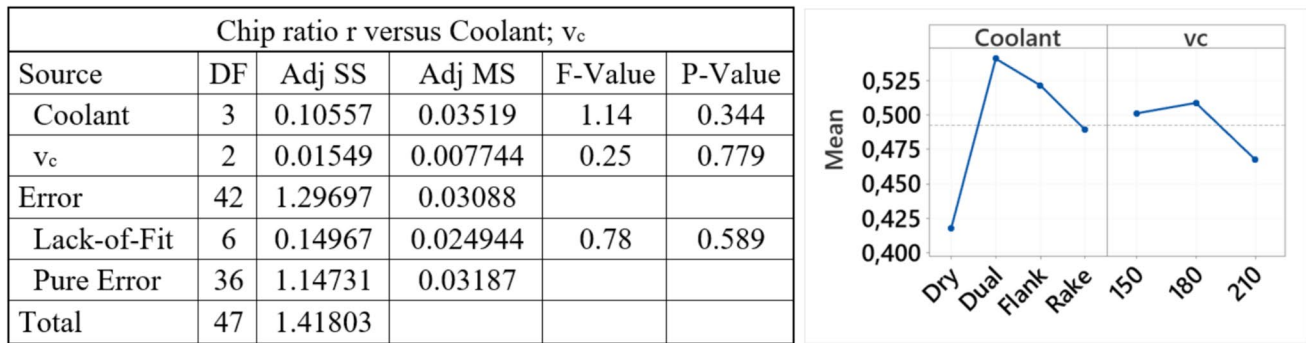


Fig. 10 ANOVA test for chip ratio with main effect plot

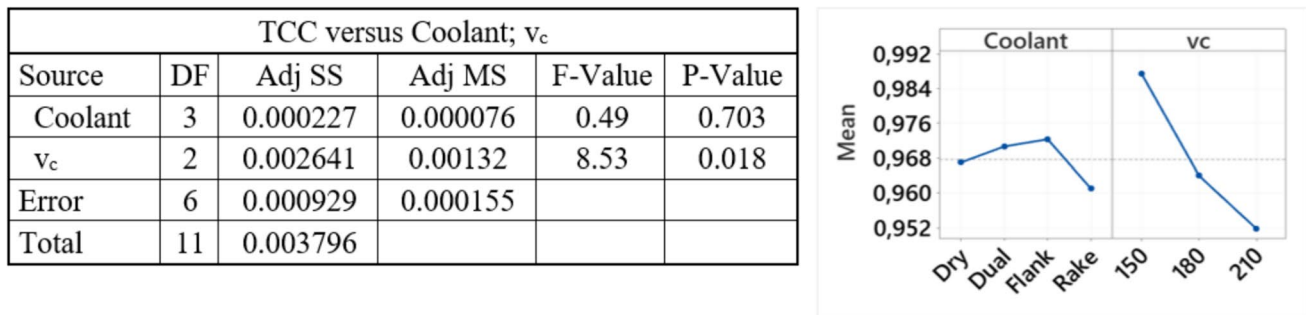


Fig. 11 ANOVA test for tool contact length with main effect plot

is not sufficiently strong, as was proven for high-pressure cooling with liquid coolants by Masek et al. [43].

The shear angle represents a measure of the chip formation efficiency. It shows the degree of material deformation and the amount of heat generated during cutting. In general, the angle increases with the speed and cutting temperature. Subsequently, a lower plastic deformation intensity occurred in the work material. The results obtained, as illustrated in Fig. 12d, demonstrate that the shear angle increased progressively with cutting speed under dry conditions; similar observations were reported in Daymi's et.al. study [44]. For an increase in speed of 40%, the angle increased at a similar rate of 50%. A higher shear angle results in a decreased shear zone area, which reduces the shear force and cutting energy. All cryo-cooling strategies demonstrated an increase in the shear angle with increasing speed. However, the increase was not progressive; hence, the cutting speed did not significantly influence the shear of the material under cryo-cooling conditions according to the ANOVA test (Fig. 13). In a given range of cutting speed, a 16% increase in shear angle can be observed in the main effect plot. This is a sign of intensive cooling of the chip and cutting region. The direction of the cooling media flow did not significantly influence the shear angle.

3.3 Microstructural analysis of workpiece and chips

The microstructural constituents of a material dictate its behavior and operational performance. Consequently, the microstructural phases of the work material were analyzed and identified, as shown in Fig. 14. The composite consisted of an α -Al matrix and reinforcing SiC particles. Primary Si particles exist in the form of polyhedral particles (2). The eutectic Mg_2Si phase (4) can be found predominantly at the edge of the Si particles and Fe-based phases (1) with either dendritic, skeletal, or partial fish-bone morphology or in the form of globular particles. Fe-rich intermetallic phases were present in the form of polyhedrons, thick needles/platelets (Fig. 14b), and irregular platelets (Fig. 14c). Thick and occasionally fragmented uniform needles were identified as the β -AlFeSi intermetallic phase, while the longer irregular platelets with Mg content were the π - Al_8Mg_3FeSi phase, and polyhedrons were α - Al_8Fe_2Si . Scattered Ti particles were occasionally found either in the α -Al matrix or near the fragmented SiC-reinforced phase.

The microstructural analyses of the workpiece material and chip after dry cutting are compared in Fig. 15a and b, respectively. The distribution of SiC particles in the ductile matrix was not uniform, and particle agglomeration with large clusters was observed across the microstructure of the

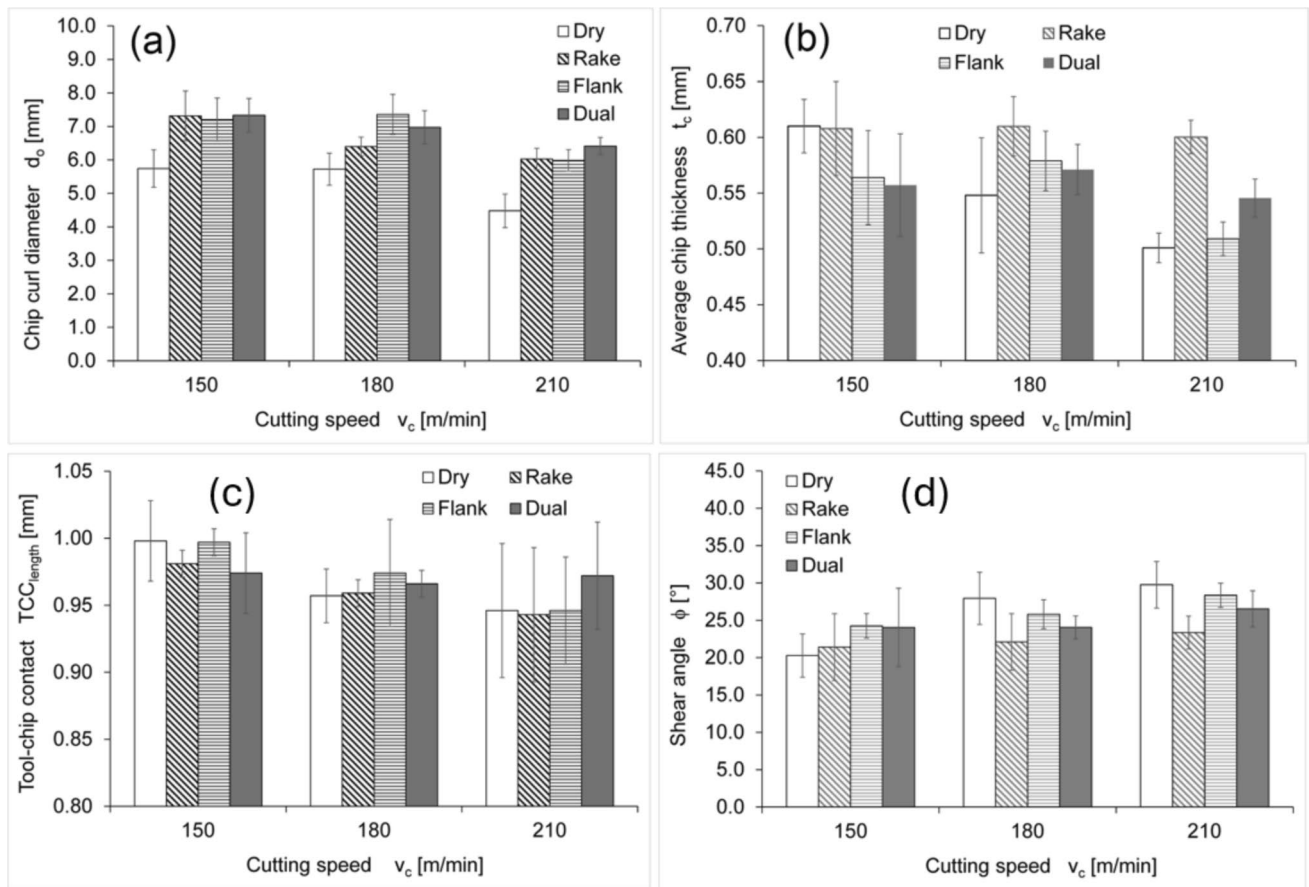


Fig. 12 Graphs of chip curl diameter (a), average chip thickness (b), TCC length (c), and chip compression ratio (d) variation with cutting speed and cooling conditions

Shear angle SA versus Coolant; v_c					
Source	DF	Adj SS	Adj MS	F-Value	P-Value
Coolant	3	57.05	19.018	0.83	0.492
v_c	2	81.43	40.716	1.79	0.196
Error	18	409.97	22.776		
Lack-of-Fit	6	49.07	8.179	0.27	0.94
Pure Error	12	360.9	30.075		
Total	23	548.46			

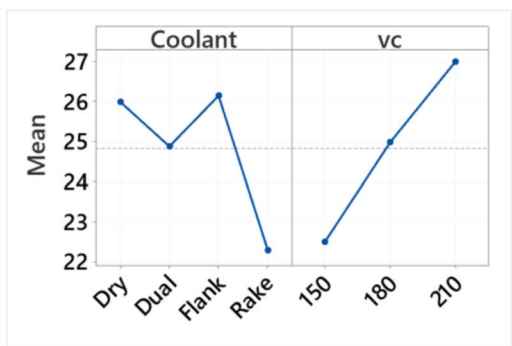
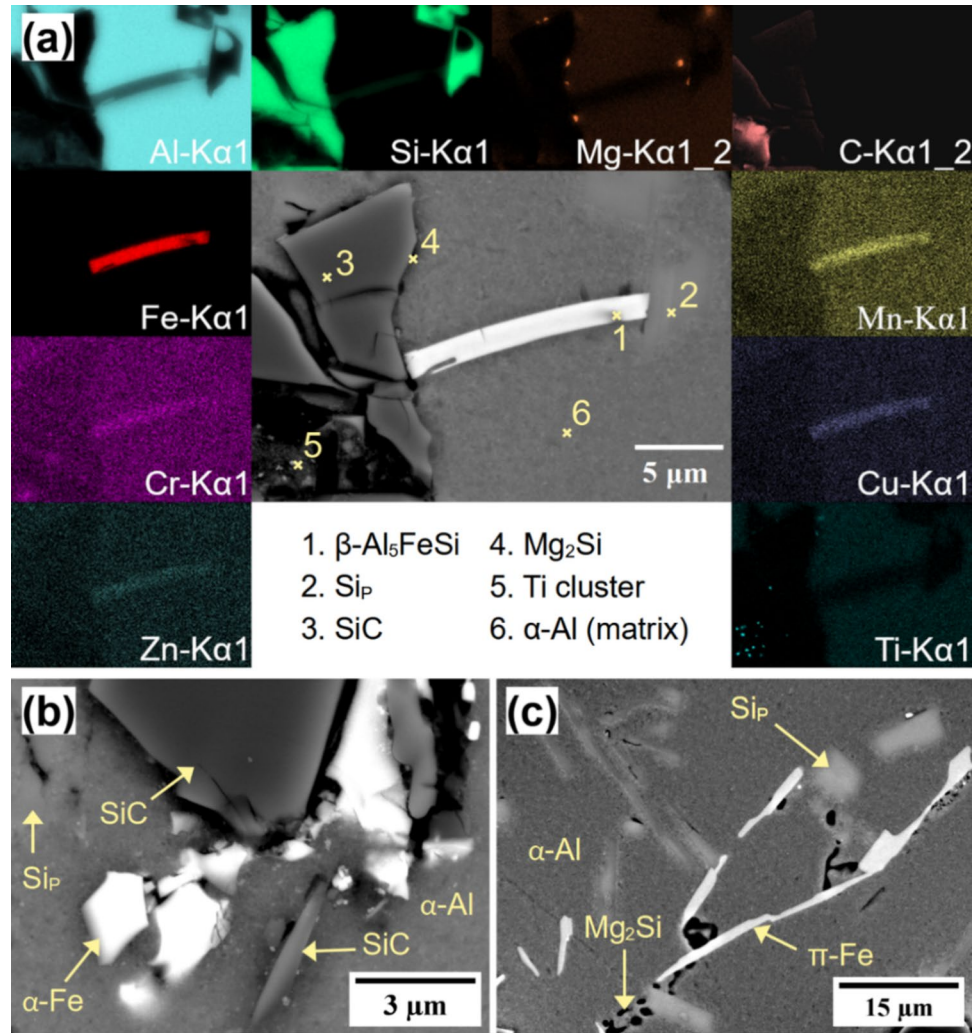


Fig. 13 ANOVA test for shear angle with main effect plot

workpiece (Fig. 15a). This arrangement leads to the presence of large areas without SiC particles, inducing anisotropy in the material properties. This significantly affects the homogeneity of plastic deformation and built-up edge formation during chip formation. The microstructure of the chips after dry-cutting exhibited smaller oriented phases ($Si_p/Mg_2Si/Fe$ -based). Moreover, a more uniform distribution of the SiC particles along the shear bands was observed. Redistribution

occurred across the thickness of the chip. This is believed to be based on the phenomena that emerge during dry machining. The heat produced is retained to a greater extent in the material. The aluminum matrix becomes softer and more fluid. Thus, the SiC particles tend to collide with one another and cluster more because the particles have a higher melting point than the aluminum matrix. However, the particles could not reach the softening state at this temperature.

Fig. 14 EDXS analysis and BSE micrographs of workpiece material: (a) element mapping of present phases, (b) detail of polyhedral α -Fe phases, (c) thickness variation of π -Fe phase



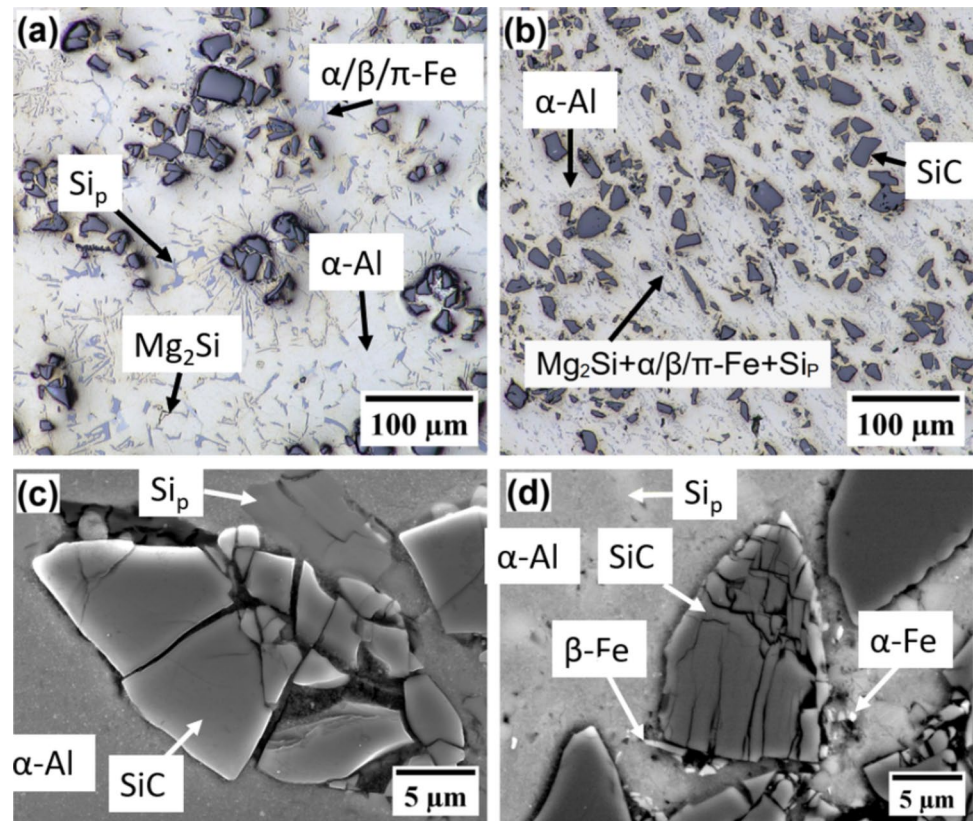
Moreover, these non-metallic particles do not form a perfectly homogenous mixture with the metallic matrix, which promotes cluster formation. Various degrees of particle fragmentation were observed in the workpiece (Fig. 15c). In comparison, fragmentation is expected to be significantly higher in chips in general, as observed under dry conditions (Fig. 15d), mainly owing to plastic deformation.

Dry cooling significantly affects the intensity of plastic deformation during chip formation. The shear band localization increased with the cutting speed. However, it created regions with more space between the SiC bands and a more compact arrangement of the $\text{Si}_\text{P}/\text{Mg}_2\text{Si}$ and Fe-based phases, as shown in Fig. 16a. This is significantly different from the particle distribution for all three cryogenic approaches. Rake cooling resulted in a similar chip morphology (Fig. 16b); however, the SiC bands were less oriented according to the shear band. Some of the undeformed α -Al rosette cells could still be observed, and the bands were accompanied by a smaller number of phase agglomerates. Plastic deformation and shear bands were less apparent (localized) in the case of

flank cooling and dual cooling. This indicates a lower temperature in the primary shear zone. Some of the SiC particles and phases did not follow the material flow, which resulted in their less uniform arrangement (Fig. 16c and d). Thus, the microstructure is more similar to that of the workpiece material, but with a more uniform distribution of SiC particles.

The mechanism of chip separation-crack initiation and propagation in the material was observed to be dominant. Chip formation is followed by the initiation of cracks along the matrix-particle interface. The formation of micro voids initially occurs at the locations of existing inhomogeneities or along the boundaries of fragmented SiC particles, and their subsequent coalescence results in the development of microcracks. The Mg_2Si and Si_P phases are obstacles that bridge microcrack propagation, whereas the hard SiC particles act as barriers and deflect the propagating cracks (Fig. 17d). However, the brittle Fe-based intermetallic exhibited fracturing, resulting in the formation of facets aligned along the boundaries of the remaining phases and SiC particles (Fig. 17c). With a growing trend towards particle

Fig. 15 Microstructure of material: (a) SiC particle and phase distribution in the workpiece (optical microscopy), (b) SiC and phase distribution in a chip (dry condition, optical microscopy), (c) fragmented SiC particle in the workpiece (SE + BSE micrograph), (d) intensive fragmentation of SiC particle in a chip (dry condition, SE + BSE micrograph)



fragmentation, these factors serve as possible precursors to the formation of cracks. The fracture resistance of a composite material depends largely on the onset and propagation of cracks. These cracks emerged not only from the unrestricted side of the chip, but also from the newly developed rear side (interface between the tool and chip) (Fig. 17a and b).

4 Conclusions

Cryogenic cooling significantly influences chip formation in aluminum–silicon carbide (A359/SiC-20wt%) compositemachining. The results show that cryogenic cooling produces shorter and less curled chips across all cutting speeds, with rake and dual cooling strategies demonstrating the best chip breakability. The chip length was decreased from 30 to 40 mm to 10 to 20 mm using cryogenic cooling. Despite minimal changes in tool-chip contact length, cryogenic cooling promotes a more uniform SiC particle distribution, reducing the shear band-induced clustering observed in dry machining.

Quantitative analysis reveals that cryogenic cooling increases chip compress ratio up to 25 % and chip curl radius up to 20%, particularly in dual cooling conditions, which contributes to improved material removal efficiency. Furthermore, cryogenic cooling stabilizes shear angles rather than increasing them, preventing excessive variations across different speeds. Cutting speed had statistically significant influence on the chip curl ratio and TCC length on the significance level of 5%. The findings also confirm that chip separation is primarily governed by crack propagation along the matrix-particle interface, leading to frayed chip edges and enhanced breakability.

These findings provide valuable insights into the role of cryogenic cooling in machining aluminum matrix composites. By optimizing cooling strategies and cutting parameters, manufacturers can improve chip control, enhance tool life, and achieve better surface quality. These advancements can contribute to more efficient and sustainable machining practices for improving the machinability of advanced composite materials.

Fig. 16 Microstructural changes and SiC particle distribution in chips based on the cooling condition ($v_c = 180$ m/min): (a) dry, (b) rake, (c) dual, and (d) flank cooling

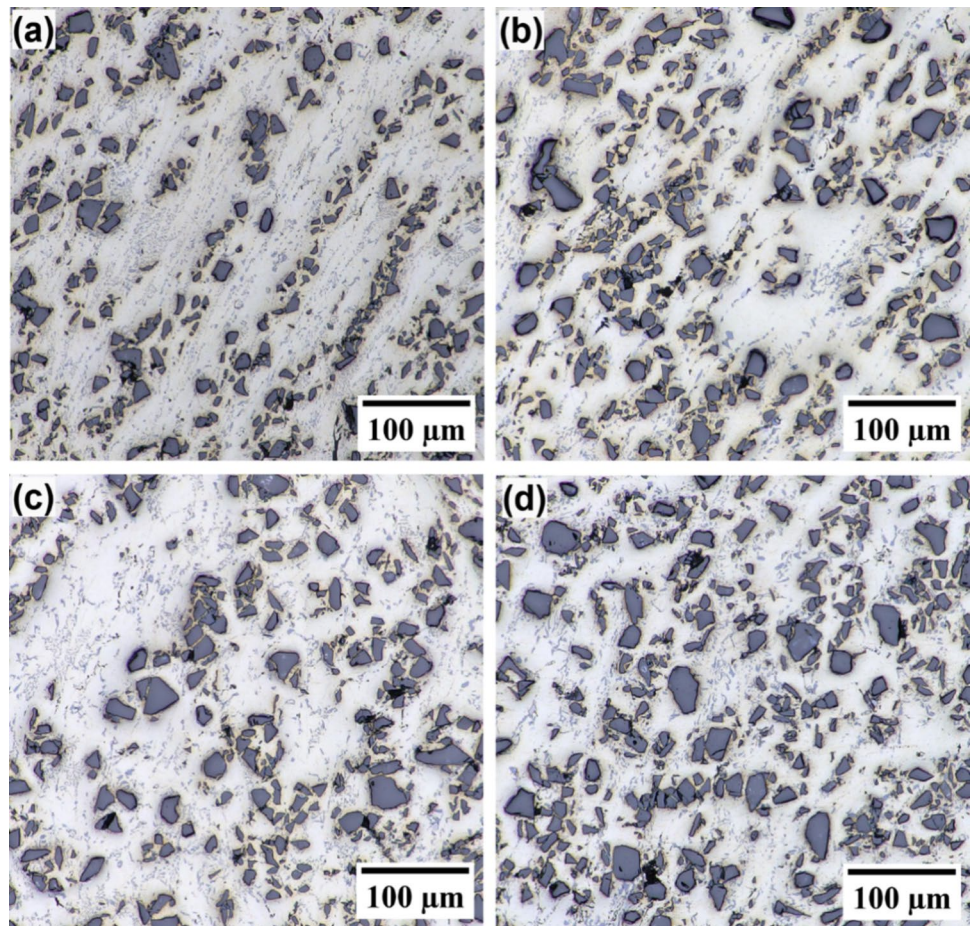
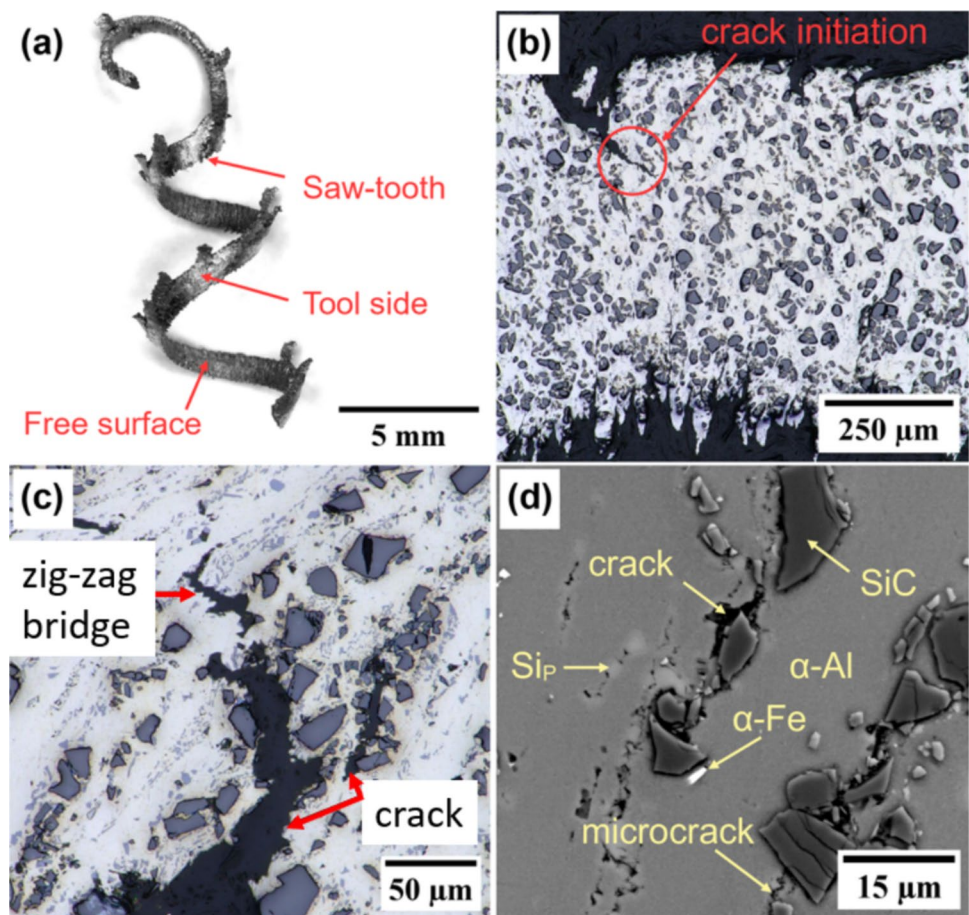


Fig. 17 Crack initiation and propagation in chips (cryo-cooling condition): (a) general view of a chip, (b) crack initiation from the tool side of the chip, (c) crack propagation from the tool side of the chip along the shear bands and zig-zag band bridging, (d) details of crack propagation along the oriented phases



Acknowledgements We would like to acknowledge funded project Next-Light; DNR: 2020-04292 with support from the strategic innovation program LIGHTer, a joint venture by Vinnova, Formas, and the Swedish Energy Agency. CryoMach (Ref. No: 2018-03332) with equipment support, a Vinnova (Swedish Government Agency for Innovation Systems), and Eureka SMART Advanced Manufacturing. Special thanks to industry partners Fortiva Tools Mr Kalle Falk and Air Liquide Mr Niklas Ehrlin and Ms Pernilla Lundberg. Open access: This publication was created with the contribution of the knowledge obtained within the project, Machine Tools and Precision Engineering (MTPE), Reg. No. CZ.02.1.01/0.0/0.0/16_026/0008404.

Author contribution Petr Mašek: writing, visualization, and editing. Nageswaran Tamil Alagan: experimental design, methodology, data analysis, writing—review and editing, and resource acquisition. Vladimír Mára: writing, data acquisition, data analysis, and visualization. Samuel A. Awe: writing—review and editing. Emeka Nwabuisi: experimental design, methodology, data acquisition, and data analysis. Pavel Zeman: methodology, writing—review and editing, resource acquisition, and data analysis.

Funding Open access publishing supported by the institutions participating in the CzechELib Transformative Agreement.

Declarations

Competing interests The authors declare no competing interests.

Open Access This article is licensed under a Creative Commons Attribution 4.0 International License, which permits use, sharing, adaptation, distribution and reproduction in any medium or format, as long as you give appropriate credit to the original author(s) and the source, provide a link to the Creative Commons licence, and indicate if changes were made. The images or other third party material in this article are included in the article's Creative Commons licence, unless indicated otherwise in a credit line to the material. If material is not included in the article's Creative Commons licence and your intended use is not permitted by statutory regulation or exceeds the permitted use, you will need to obtain permission directly from the copyright holder. To view a copy of this licence, visit <http://creativecommons.org/licenses/by/4.0/>.

References

- Przestacki D, Szymanski P, Wojciechowski S (2016) Formation of surface layer in metal matrix composite A359/20SiCP during laser assisted turning. *Compos Part Appl Sci Manuf* 91:370–379. <https://doi.org/10.1016/j.compositesa.2016.10.026>
- Wu Q, Xu W, Zhang L (2019) Microstructure-based modelling of fracture of particulate reinforced metal matrix composites. *Compos Part B Eng* 163:384–392. <https://doi.org/10.1016/j.compositesb.2018.12.099>
- Baker A, Dutton S, Kelly D (2004) *Composite materials for aircraft structures*, 2 AIAA. Reston, Virginia

4. Gay D (2014) Composite materials: design and applications, 3 CRC Press. Boca Raton. <https://doi.org/10.1201/b17106>
5. Harris B (1999) Engineering composite materials, 2 Institute of Materials. London
6. Masek P, Zeman P, Kolar P (2021) Cutting temperature measurement in turning of thermoplastic composites using a tool-work thermocouple. *Int J Adv Manuf Technol* 116:3163–3178. <https://doi.org/10.1007/s00170-021-07588-0>
7. Masek P, Zeman P, Kolar P, Holesovsky F (2019) Edge trimming of C/PPS plate. *Int J Adv Manuf Technol* 101:157–170. <https://doi.org/10.1007/s00170-018-2857-1>
8. Behun M, Gavurova B, Tkacova A, Kotaskova A (2018) The impact of the manufacturing industry on the economic cycle of European Union countries. *J Compet* 10:23–39. <https://doi.org/10.7441/joc.2018.01.02>
9. Chawla N, Shen Y-L (2001) Mechanical behavior of particle reinforced metal matrix composites. *Adv Eng Mater* 3:357–370. [https://doi.org/10.1002/1527-2648\(200106\)3:6%3c357::AID-ADEM357%3e3.0.CO;2-I](https://doi.org/10.1002/1527-2648(200106)3:6%3c357::AID-ADEM357%3e3.0.CO;2-I)
10. Chen J-P, Gu L, He G-J (2020) A review on conventional and nonconventional machining of SiC particle-reinforced aluminium matrix composites. *Adv Manuf* 8:279–315. <https://doi.org/10.1007/s40436-020-00313-2>
11. Dandekar CR, Shin YC (2012) Modelling of machining of composite materials: a review. *Int J Mach Tools Manuf* 57:102–121. <https://doi.org/10.1016/j.jmactools.2012.01.006>
12. Laghari RA, Jamil M, Hussain MI, Gupta MK, Krolczyk GM (2023) A state-of-the-art review on recently developed sustainable and green cooling/lubrication technologies in machining metal matrix composites (MMCs). *Int J Precision Eng Manuf-Green Technol* 10:1637–1660. <https://doi.org/10.1007/s40684-023-00521-8>
13. Chen J, Gu L, Zhao W, Guagliano M (2021) Simulation of temperature distribution and discharge crater of SiCp/Al composites in a single-pulsed arc discharge. *Chinese J Aeronaut* 34(9):37–46. <https://doi.org/10.1016/j.cja.2020.05.033>
14. Repeto D, Fernández-Vidal SR, Mayuet PF, Salguero J, Batista M (2020) On the machinability of an Al-63%SiC metal matrix composite. *Materials* 13(5):1186. <https://doi.org/10.3390/ma13051186>
15. Hung NP, Yeo SH, Lee KK, Ng KJ (1998) Chip formation in machining particle-reinforced metal matrix composites. *Mater Manuf Process* 13:85–100. <https://doi.org/10.1080/10426919808935221>
16. Sivalingam V et al (2023) Understanding the machining characteristics of Al6082 hybrid metal matrix composites milled under cryogenic cooling conditions. *Int J Adv Manuf Technol* 129:3387–3402. <https://doi.org/10.1007/s00170-023-12534-3>
17. Laghari et al (2023) Investigating the tribological aspects of tool wear mechanism and tool life in sustainable lubri-cooling face milling process of particle-reinforced SiCp/Al metal matrix composites. *IMECE2022*–95183. <https://doi.org/10.1115/IMECE2022-95183>
18. Khanna N, Agrawal C, Pimenov DY, Singla AK, Machado AR, da Silva LRR, Gupta MK, Sarikaya M, Krolczyk GM (2021) Review on design and development of cryogenic machining setups for heat resistant alloys and composites. *J Manuf Process* 68:398–422. <https://doi.org/10.1016/j.jmapro.2021.05.053>
19. Duan C, Sun W, Che M, Yin W (2019) Effects of cooling and lubrication conditions on tool wear in turning of Al/SiCp composite. *Int J Adv Manuf Technol* 103:1467–1479. <https://doi.org/10.1007/s00170-019-03565-w>
20. Josyula SK, Narala SKR, Charan EG, Kishawy HA (2016) Sustainable machining of metal matrix composites using liquid nitrogen. *Proc CIRP* 40:568–573. <https://doi.org/10.1016/j.procir.2016.01.135>
21. Aurich JC, Zimmermann M, Schindler S, Steinmann P (2016) Turning of aluminum metal matrix composites: influence of the reinforcement and the cutting condition on the surface layer of the workpiece. *Adv Manuf* 4:225–236. <https://doi.org/10.1007/s40436-016-0152-7>
22. Ghoreishi R, Roohi AH, Ghadikolaei AD (2019) Evaluation of tool wear in high-speed face milling of Al/SiC metal matrix composites. *J Braz Soc Mech Sci Eng* 41:146. <https://doi.org/10.1007/s40430-019-1649-3>
23. Chakravarthy VV, Rajmohan T, Vijayan D, Palanikumar K (2022) Sustainable drilling of nano SiC reinforced Al matrix composites using MQL and cryogenic cooling for achieving the better surface integrity. *Silicon* 14:1787–1805. <https://doi.org/10.1007/s12633-021-00977-w>
24. Abbas CA, Huang C, Wang J, Wang Z, Liu H, Zhu H (2020) Machinability investigations on high-speed drilling of aluminum reinforced with silicon carbide metal matrix composites. *Int J Adv Manuf Technol* 108:1601–1611. <https://doi.org/10.1007/s00170-020-05409-4>
25. Lin JT, Bhattacharyya B, Ferguson WG (1998) Chip formation in the machining of SiC-particle-reinforced aluminium-matrix composites. *Compos Sci Technol* 58:285–291. [https://doi.org/10.1016/S0266-3538\(97\)00126-7](https://doi.org/10.1016/S0266-3538(97)00126-7)
26. Sadat AB (2009) On the quality of machined surface region when turning *al/sic* metal matrix composites. *Mach Sci Technol* 13:338–355. <https://doi.org/10.1080/10910340903237731>
27. Abbas AC, Huang C, Li B, Liu H (2024) Research on cryogenic high-speed drilling performance of metal matrix composite materials (Al/SiC) using cryogenically treated drills. *J Braz Soc Mech Sci Eng* 46:448. <https://doi.org/10.1007/s40430-024-05007-5>
28. Manna A, Bhattacharaya B (2005) Influence of machining parameters on the machinability of particulate reinforced Al/SiC-MMC. *Int J Adv Manuf Technol* 25:850–856. <https://doi.org/10.1007/s00170-003-1917-2>
29. Chintada S, Dora SP, Prathipati R (2019) Investigations on the machinability of Al/SiC/RHA hybrid metal matrix composites. *Silicon* 11:2907–2918. <https://doi.org/10.1007/s12633-019-0080-9>
30. Muthukrishnan M, Murugan M, Prahada Rao K (2008) Machinability issues in turning of Al-SiC (10p) metal matrix composites. *Int J Adv Manuf Technol* 39:211–218. <https://doi.org/10.1007/s00170-007-1220-8>
31. Xiang J, Xie L, Gao F (2021) Modeling high-speed cutting of SiCp/Al composites using a semi-phenomenologically based damage model. *Chinese J Aeronaut* 34(8):218–229. <https://doi.org/10.1016/j.cja.2020.09.001>
32. Nakayama K (1962) A study on chip-breaker. *Bull JSME* 5:142–150. <https://doi.org/10.1299/jsme1958.5.142>
33. Sandvik Coromant (2021) Cutting tool materials, <https://www.sandvik.coromant.com/en-us/knowledge/materials/pages/cutting-tool-materials.aspx>. Accessed 11 July 2024
34. Dabade UA, Joshi SS (2009) Analysis of chip formation mechanism in machining of Al/SiCp metal matrix composites. *J Mater Process Technol* 209:4704–4710. <https://doi.org/10.1016/j.jmatprotec.2008.10.057>
35. Wu Q, Xu W, Zhang L (2019) Machining of particulate-reinforced metal matrix composites: an investigation into the chip formation and subsurface damage. *J Mater Process Technol* 274. <https://doi.org/10.1016/j.jmatprotec.2019.116315>
36. Tamil Alagan N, Zeman P, Hoier P, Beno T, Klement U (2019) Investigation of micro-textured cutting tools used for face turning

- of alloy 718 with high-pressure cooling. *J Manuf Process* 37:606–616. <https://doi.org/10.1016/j.jmapro.2018.12.023>
37. Tamil Alagan N, Zeman P, Mara V, Beno T, Wretland A (2021) High-pressure flank cooling and chip morphology in turning Alloy 718. *CIRP J Manuf Sci Technol* 35. <https://doi.org/10.1016/j.cirpj.2021.08.012>
38. Shaw MC (2008) *Metal cutting principles*. 2nd edition. Publisher: Oxford University Press, ISBN 978-0195142068
39. Yaman K, Tekiner Z (2024) Investigation of the effect of built-up edge on chip morphology at the cutting edge during turning operation. *J Polytech*. <https://doi.org/10.2339/politeknik.1432815>
40. Kaynak Y, Gharibi A, Yilmaz U, Koklu U, Aslantas K (2024) A comparison of flood cooling, minimum quantity lubrication, and high-pressure coolant on machining and surface integrity of titanium Ti-5553 alloy. *J Polytech*. <https://doi.org/10.1016/j.jmapro.2018.06.003>
41. Astakhov V, Shvets S (2004) The assessment of plastic deformation in metal cutting. *J Mater Process Technol* 146:193–202. <https://doi.org/10.1016/j.jmatprotec.2003.10.015>
42. Storchak M, Drewle K, Menze C, Stehle T, Mohring H-C (2022) Determination of the tool–chip contact length for the cutting processes. *Materials* 15(9):3264. <https://doi.org/10.3390/ma15093264>
43. Masek P, Maly J, Zeman P, Heinrich P, Tamil Alagan N (2022) Turning of titanium alloy with PCD tool and high-pressure cooling. *J Manuf Process* 84:871–885. <https://doi.org/10.1016/j.jmapro.2022.10.034>
44. Daymi A, Boujelbene M, Salem SB, Hadj Sassi B, Torbaty S (2009) Effect of cutting speed on chip morphology and cutting force. *Arch Comput Mater Sci Surf Eng* 1(2):77–83

Publisher's Note Springer Nature remains neutral with regard to jurisdictional claims in published maps and institutional affiliations.